Superconducting Phases of Phosphorus Hydride Under Pressure: Stabilization via Mobile Molecular Hydrogen

*Tiange Bi, Dan Miller, Andrew Shamp, Eva Zurek**

Department of Chemistry, State University of New York at Buffalo, Buffalo, NY 14260-3000, USA

E-mail: ezurek@buffalo.edu

At 80 GPa phases with the PH_2 stoichiometry, which are composed of simple cubic like phosphorus layers capped with hydrogen atoms and layers of H_2 molecules, are predicted to be important species contributing to the recently observed superconductivity in compressed phosphine. The electron phonon coupling in these phases results from the motions of the phosphorus atoms and the hydrogens bound to them. The role of the mobile H_2 layers is to decrease the Coulomb repulsion between the negatively charged hydrogen atoms capping the phosphorus layers. An insulating PH_5 phase, whose structure and bonding is reminiscent of diborane, is also predicted to be metastable at this pressure.

Pressure can have a dramatic effect on structure, chemical bonding, reactivity, and the properties of matter.[1–4] High pressure experiments have recently led to the discovery of superconductivity in hydrides of two p-elements: sulfur[5] and phosphorus.[6] Density functional theory (DFT) calculations predicted that phases with the H_3S stoichiometry would become more stable than superconducting solid H_2S[7] and solid H_2 at ∼6 GPa,[8] and the T_c of an $Im\bar{3}m$-H_3S phase estimated using the Allen-Dynes modified McMillan equation, ∼200 K at 200 GPa,[9] was in good agreement with the experimental observations.[5] These successes inspired the search for superconductivity in compressed phosphine.[6] Experiments showed metalization at ∼30 GPa, and the measured resistance disappeared at 83 GPa and 30 K. The T_c increased with increasing pressure, reaching 103 K at 207 GPa. The lack of experimental structural information motivated a series of theoretical predictions that identified several phases, including PH,[10] PH_2,[10,11] and PH_3[10,12] as candidates for the experimentally observed superconductivity between 100 and 200 GPa. Notably, all of the reported structures were found to be metastable, that is they were thermodynamically unstable with respect to the elemental phases, but phonon calculations confirmed they were local minima.

Because the aforementioned studies[10–13] did not carefully investigate the PH_n phase diagram for pressures less than 100 GPa, herein we have carried out an exploration of the potential energy surface (PES) for $n = 1 - 6$ using the evolutionary algorithm XTALOPT[14] at 40, 50, 80 and 100 GPa. The enthalpies of formation, ΔH_F, of the metastable phases ranged from 15 to 55 meV/atom with respect to the elemental phases. Because no structural transitions were found to occur in the most stable phases with $n = 1 - 4, 6$ below 100 GPa, and the superconductivity was first observed at 83 GPa, we focus on the results obtained at 80 GPa. Some of the structures found at 100 GPa have been reported previously.[10–12]

Except for PH_5, the most stable structures were metallic, and they were composed of simple cubic (sc) like layers of phosphorus, with the atoms in the top and bottom layers terminated by hydrogen atoms; an example is the PH_2 phase shown in Fig. 1. At this pressure phosphorus possesses a sc structure.[15] The two-dimensional lattices were separated by layers of H_2 molecules. The number of layers of phosphorus/H_2 were 6/2, 4/3, 4/5, 2/3 and 2/5 for the most stable PH, PH_2, PH_3, PH_4 and PH_6 phases found, respectively. Below 63 GPa the most stable PH_5 phase also adopted this type of structural motif with two P-H layers separated by four H_2 layers. However, at 80 GPa the most stable system was a non-metallic PH_5 phase whose structure and electronic structure resemble that of diborane, with its electron deficient three-center-two-electron (3c-2e) bonds. With the exception of a Cm-PH phase, by 100 GPa the most stable phases were no longer layered.

Herein, an in-depth analysis of the dynamically stable PH_2 phases with $Cmmm$ and $C2/m$ symmetry, one of which is illustrated in Fig. 1, are provided as an example to demonstrate the properties of the layered structures. These systems were chosen because: (i) their estimated T_cs provided the best agreement with the experimental results; (ii) the reactions $2PH \rightarrow PH_2 + P$ and $PH_3 \rightarrow PH_2 + \frac{1}{2}H_2$ are exothermic with enthalpies of -6.4 and -8.6 meV/atom at 80 GPa, respectively. Our detailed analysis reveals that even though the freely-rotating H_2 molecules are not important for the superconducting properties of these phases, they stabilize them by decreasing the Coulomb repulsion between the -PH atoms from adjacent layers.

In $Cmmm$-PH_2 two of the H_2 layers, those closest to the -PH atoms, are parallel to the a-axis whereas the third is parallel to the b-axis. The phosphorus atoms are octahedrally coordinated.

The electron localization function confirmed the presence of P-P, P-H and H-H bonds. Our evolutionary searches identified another dynamically stable PH_2 phase with $C2/m$ symmetry that was nearly isoenthalpic with $Cmmm$. In the $C2/m$ phase, which is shown in Fig. 2, the P-P-H angles were 179.4° (vs. 180° for $Cmmm$) and the H_2s closest to the P-H atoms were tilted with an angle of 19.5° to the a-axis, resulting in a slightly smaller volume and a 5.1 meV/atom smaller PV contribution to the enthalpy.

The nudged elastic band method estimated a barrier of 3.1 meV/atom for a pathway connecting the $Cmmm$ and $C2/m$ phases that consisted of the concerted rotation of all of the H_2 molecules in the structure, and was employed to determine the barrier for a 180° rotation of the H_2s in the middle layer (12.4 meV/atom), the top and bottom layers (6.9 meV/atom), and all three layers (6.1 meV/atom). To investigate the mobility of the H_2s further, molecular dynamics (MD) calculations were carried out at 15, 30, 100, and 300 K. In all of the simulations free rotation of H_2 was observed, and hydrogen atoms were exchanged between the H_2 and P-H units. This behavior is akin to the proton transfer between the H_2 molecules within the graphite-like layers of Phase-IV of solid H_2, which occurs during their rotation as observed in MD simulations.[17] Moreover, below 110 GPa the low-pressure phase I of solid hydrogen consists of freely rotating molecules on a hexagonal closed-packed lattice.[16] At times the rotations in our MD simulations resulted in the molecules comprising the central layer to come close enough to each other so that extended hydrogenic networks with H-H distances of ∼0.8-1.0 Å formed and these lattices appeared to "flow". However, when the geometries were optimized at 0 K the hydrogenic lattices broke and the H_2 molecules reformed.

The Bader charges of both of the PH_2 phases showed that the phosphorus atoms that only formed P-P bonds and the H_2 hydrogens were nearly neutral. The average charge on the phosphorus and hydrogen atoms within the P-H units were +0.38 and -0.40, respectively. We therefore postulated that the role of the H_2 layers within the structure was to reduce the Coulomb repulsion between the negatively charged hydrogens in the P-H groups via screening, and by increasing the P-H$\cdots$H-P separation.

To test this hypothesis the $C2/m$-PH_2 phase was modified by varying the number of H_2 layers and the resulting structures were optimized at 80 GPa. As shown in Fig. 2, removal of all of the H_2 layers in a geometry that staggered the P-H contacts resulted in a P_2H structure whose ΔH_F was 80.4 meV/atom less stable than the parent. Modification of the structure so that the P-H groups directly pointed towards each other destabilized the system by a further 85.2 meV/atom. The internal energy of the staggered system was 30.4 meV/atom larger, but its PV contribution to the enthalpy was 115.6 meV/atom smaller. This suggests that the increased Coulomb repulsion stemming from the shorter P-H$\cdots$H-P distances in the staggered phase (0.956 Å vs. 1.215 Å) is outweighed by its smaller volume (47.25 Å^3/unit cell vs. 48.64 Å^3/unit cell). P_2H_3 and the most stable PH phase were derived from the unstaggered P_2H wherein H_2s were added in the voids between the P-H motifs. Both of their ΔH_F values were smaller than that of the P_2H parent. A PH structure wherein the layers containing P-H units were staggered was not a stationary point on the PES. Addition of one more H_2 layer to $C2/m$-PH_2 yields a P_2H_5 phase whose ΔH_F was the same as that of PH_2, suggesting that further addition of H_2 would yield similarly stable structures.

The bands and DOS of both of the PH_2 phases were nearly free electron like, and their metallicity was due primarily to phosphorus p-states. The hydrogen exchange observed in the MD

simulations illustrates that the vibrations involving hydrogen atoms are strongly anharmonic, suggesting that anharmonicity is also likely to be important for an accurate determination of the T_c. To obtain a rough estimate of the T_c we employed the Allen-Dynes modified McMillan equation, see Table 1. The T_c for PH_3 was not calculated because we were unable to find a phase with this stoichiometry that was dynamically stable at 80 GPa, using cells that contained up to 20 formula units.

The T_cs of the two PH_2 phases yielded the best agreement with experiment, 30 K at 83 GPa.[6] Our results are closer to experiment than those previously obtained using DFT for superconductors, wherein an $I4/mmm$ symmetry structure that did not contain layers of molecular H_2 units, and was the lowest enthalpy PH_2 phase above 153 GPa,[11] had a T_c of nearly 50 K between 75-125 GPa.[10] Interestingly, the modes that give the largest contribution towards λ within the two 80 GPa PH_2 phases originate from the vibrations of the phosphorus atoms ($<$500 cm^{-1}) and from the phosphorus-hydrogen motions ($\sim$500-2500 cm^{-1}), whereas the hydrogen vibron only furnishes a minor amount to λ. This is in contrast to the findings for the 200 GPa PH_2 phases, which did not contain molecular H_2 units, wherein λ(H-H) was larger that λ(P-P).[11]

The T_c of phosphorus is 4.3 K at 70 GPa, and it decreases below 4 K up to 160 GPa.[18] λ(P-P) is significantly smaller for the polyhydrides than for pure phosphorus. The smallest value is for PH_4, likely because its phosphorus layer is only two atoms thick such that each phosphorus atom is coordinated to one hydrogen atom. This, coupled with its decreased λ(P-H) (as compared to the other hydrides) results in a nearly negligible T_c for PH_4. A comparison of the PH and PH_2 phases shows that the increased λ of the latter is due to vibrations between 0-2000 cm^{-1}. These correspond to P-P and P-H motions, but do not include the P-H stretching mode found near $\sim$2300 cm^{-1}. This suggests that there may be an optimal thickness of the phosphorus layers that maximize the sum of the electron phonon coupling contributions arising from the H-capped phosphorus layers, and that the H_2 molecules are not important for the superconductivity. The band structures of the PH_2 phases show numerous nearly parallel steep bands that cross E_F and flat bands near Γ, in-line with the steep band/flat band scenario observed in many superconductors,[19] including H_3S.

Finally, let us take a look at the PH_n structure with the lowest ΔH_F discovered at 80 GPa: a dynamically stable $P\bar{1}$-PH_5 phase. As show in Fig. 3, it was comprised of P_2H_{10} building blocks that resemble diborane. Analogous to diborane, four out of the five valence electrons of phosphorus participate in conventional 2c-2e bonds with the terminal hydrogen atoms in P_2H_{10}, leaving four electrons in the P_2H_2 ring to participate in 3c-2e bonding. The optimized geometry of the P_2H_{10} molecule in the gas phase, Fig. 3(b), confirms that the bridging P-H bonds are weaker than the terminal P-H bonds, and the molecule attains D_{2h} symmetry, again in-line with the findings for diborane. As illustrated in Fig. 3(d), the six gas phase molecular orbitals (MOs) of P_2H_{10} that are lowest in energy resemble the HOMO (highest occupied MO) to the HOMO-5 of diborane, and the four occupied MOs of P_2H_{10} that are highest in energy have the same nodal structure as the unoccupied MOs of diborane that are shown.

Ashcroft proposed that metalization of hydrogen, whether it be in the atomic or molecular form, can be hastened via the "chemical precompression" that occurs when hydrogen is combined with, for example, a main group metal.[20] And he argued that such hydrides could be high temperature superconductors for the same reasons believed to be important for metallic hydrogen.

Indeed, vibrations that include the motions of the hydrogen atoms are the main contributors to the electron phonon coupling, λ, of the $Im\bar{3}m$-H_3S phase.[9] Herein, we have shown that hydrogen plays a very different role in two metastable PH_2 phases at 80 GPa. Layers of H_2 molecules that can rotate freely, and form mobile extended hydrogenic networks at finite temperature, reduce the Coulomb repulsion between the negatively charged hydrogens that cap simple cubic like layers of phosphorus atoms. But, the metallicity and λ of the PH_2 phases originates within the hydrogen capped phosphorus layers.

Acknowledgements

We acknowledge the NSF (DMR-1505817) for financial, and the Center for Computational Research (CCR) at SUNY Buffalo for computational support. A.S. and T.B. acknowledge financial support from the Department of Energy National Nuclear Security Administration under Award Number DE-NA0002006. D.M. was funded by the NSF (HRD-1345163).

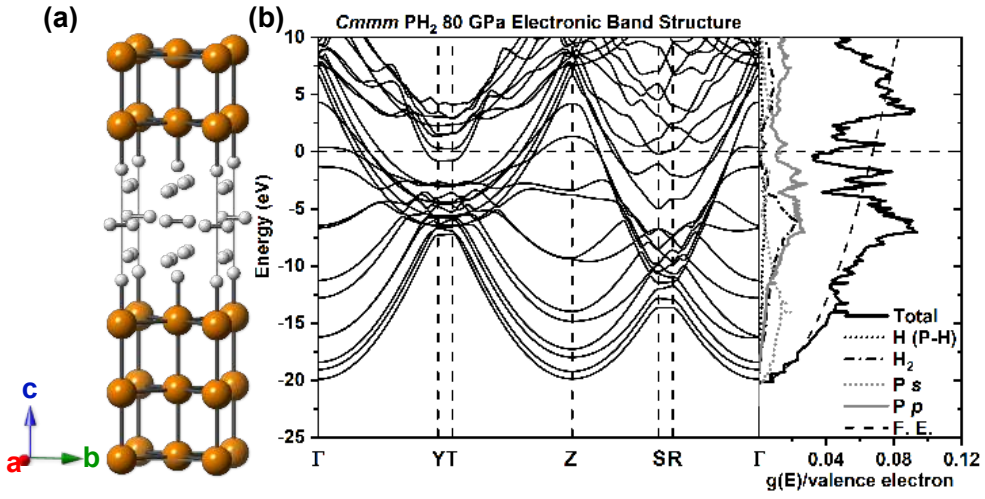

Figure 1: (a) The conventional cell of the $Cmmm$-PH_2 structure at 80 GPa. (b) Electronic band structure along with the total and site projected electronic densities of states (DOS). The Fermi level, E_F, is set to zero. The free electron (FE) DOS is given by the dashed line.

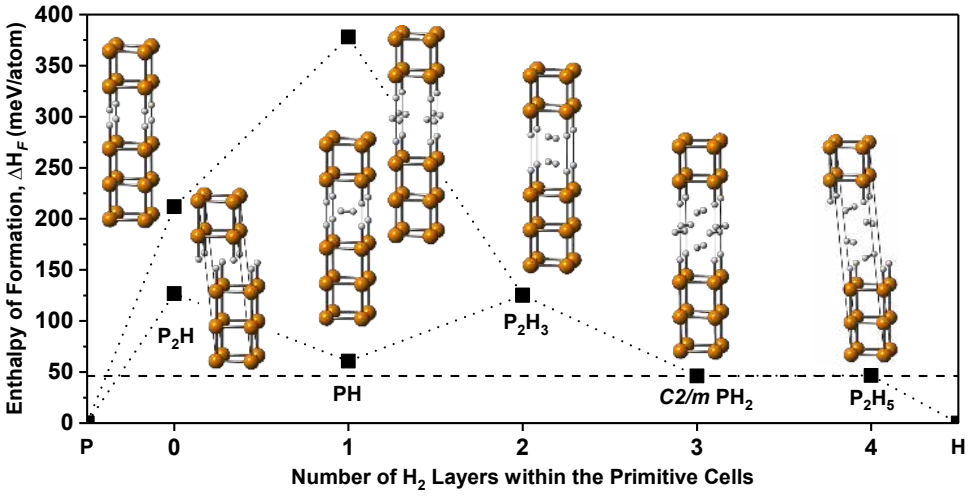

Figure 2: ΔH_F for the reaction $\mathrm{P} + \frac{n}{2}(\mathrm{H_2}) \rightarrow \mathrm{PH}_n$ versus the number of molecular hydrogen layers within $C2/m$-PH_2 and the illustrated modifications at 80 GPa. The dashed line indicates the ΔH_F of the $C2/m$-PH_2 phase. The most stable PH phase shown in this Figure had 4/1 phosphorus/H_2 layers and it was 19.3 meV/atom *less* stable than a 6/2 layer phase found in the evolutionary search.

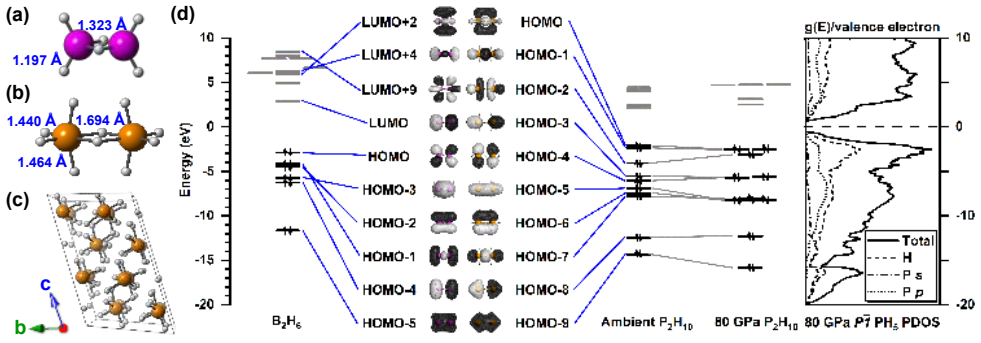

Figure 3: The optimized geometry of molecular (a) B_2H_6 and (b) P_2H_{10}. The B-H and P-H distances are provided. (c) A 2×2×2 supercell of the $P\bar{1}$-PH_5 structure at 80 GPa. (d) (From left to right) The MO level diagrams for: molecular B_2H_6 and P_2H_{10} optimized at 1 atm, and in the geometry it adopts in $P\bar{1}$-PH_5 at 80 GPa. The Fermi levels are set to 0 eV. Isosurfaces (isovalues 0.02-0.04 a.u.) of select orbitals are provided. The calculated site-projected densities of states (PDOS) of $P\bar{1}$-PH_5 at 80 GPa is located on the far right.

Table 1: Electron-phonon coupling parameter (λ), logarithmic average of phonon frequencies ($\omega_{\log}$) and estimated superconducting critical temperature (T_c) for values of the Coulomb pseudopotential (μ^*) of 0.1 for simple cubic (S.C.) phosphorous, and various PH_n phases at 80 GPa. The number of layers of phosphorus/H_2 are also provided.

System	λ	λ (P-P)	λ (P-H)	λ (H-H)	$\omega_{\log}$ (K)	T_c (K)	P/H_2
S.C. P	0.70	0.70	0	0	528.2	18.5[a]	∞/0
$C2$ PH	0.63	0.28	0.33	0.02	476.7	12.3	6/2
$C2/m$ PH_2	0.95	0.41	0.51	0.03	467.2	30.1	4/3
$Cmmm$ PH_2	0.88	0.37	0.48	0.02	529.4	29.5	4/3
$C2/m$ PH_4	0.34	0.08	0.24	0.02	683.2	1.9	2/3

[a] A value of $\mu^* = 0.18$ yields 8.2 K.

References

[1] W. Grochala, R. Hoffmann, J. Feng, N. W. Ashcroft, *Angew. Chem. Int. Ed.* **2007**, *46*, 3620–3642.

[2] M. Miao, R. Hoffmann, J. Botana, I. I. Naumov, R. J. Hemley, *Angew. Chem. Int. Ed.* **2017**, *129*, 992–995.

[3] E. Zurek, W. Grochala, *Phys. Chem. Chem. Phys.* **2015**, *17*, 2917–2934.

[4] J. Botana, X. Wang, C. Hou, D. Yan, H. Lin, Y. Ma, M. Miao, *Angew. Chem. Int. Ed.* **2015**, *54*, 9280–9283.

[5] A. Drozdov, M. Eremets, I. Troyan, V. Ksenofontov, S. Shylin, *Nature* **2015**, *525*, 73–76.

[6] A. Drozdov, M. Eremets, I. Troyan, *arXiv preprint* **2015**, arXiv:1508.06224.

[7] Y. Li, J. Hao, H. Liu, Y. Li, Y. Ma, *J. Chem. Phys.* **2014**, *140*, 174712.

[8] Y. Li, L. Wang, H. Liu, Y. Zhang, J. Hao, C. J. Pickard, J. R. Nelson, R. J. Needs, W. Li, Y. Huang, I. Errea, M. Calandra, F. Mauri, Y. Ma, *Phys. Rev. B* **2016**, *93*, 020103.

[9] D. Duan, Y. Liu, F. Tian, D. Li, X. Huang, Z. Zhao, H. Yu, B. Liu, W. Tian, T. Cui, *Sci. Rep.* **2014**, *4*, 6968.

[10] J. A. Flores-Livas, M. Amsler, C. Heil, A. Sanna, L. Boeri, G. Profeta, C. Wolverton, S. Goedecker, E. K. U. Gross, *Phys. Rev. B* **2016**, *93*, 020508.

[11] A. Shamp, T. Terpstra, T. Bi, Z. Falls, P. Avery, E. Zurek, *J. Am. Chem. Soc.* **2016**, *138*, 1884–1892.

[12] H. Liu, Y. Li, G. Gao, J. S. Tse, I. I. Naumov, *J. Phys. Chem. C* **2016**, *120*, 3458–3461.

[13] Y. Fu, X. Du, L. Zhang, F. Peng, M. Zhang, C. J. Pickard, R. J. Needs, D. J. Singh, W. Zheng, Y. Ma, *Chem. Mater.* **2016**, *28*, 1746–1755.

[14] D. C. Lonie, E. Zurek, *Comput. Phys. Commun.* **2011**, *182*, 372–387.

[15] Y. Akahama, M. Kobayashi, H. Kawamura, *Phys. Rev. B* **1999**, *59*, 8520.

[16] P. L. Loubeyre, R. Letoullec, D. Hausermann, M. Hanfland, R. J. Hemley, H. K. Mao, L. W. Finger, *Nature* **1996**, *383*, 702–704.

[17] H. Liu, Y. Ma, *Phys. Rev. Lett.* **2013**, *110*, 025903.

[18] M. Karuzawa, M. Ishizuka, S. Endo, *J. Phys.: Condens. Matter* **2002**, *14*, 10759.

[19] A. Simon, *Angew. Chem. Int. Engl.* **1997**, *36*, 1788–1806.

[20] N. W. Ashcroft, *Phys. Rev. Lett.* **2004**, *92*, 187002 (1–4).

Keywords: density functional calculations, electronic structure, high pressure chemistry, superconductors.

Table of Contents Graphic:

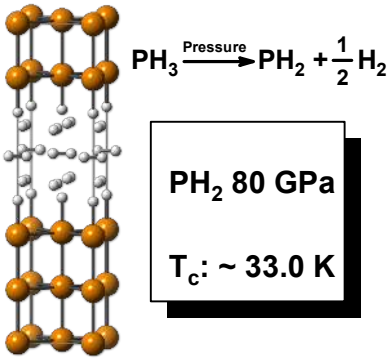

Table of Contents Text:

Superconducting Main Group Hydrides: Theoretical calculations predict that a two-dimensional superconductor composed of layers of phosphorus atoms that are capped with hydrogen atoms can be synthesized by 80 GPa. Key to the stability of this phase are layers of fluid hydrogen molecules that lie between 2D sheets and minimize the Coulomb repulsion between them. Such a phase may be responsible for the recently observed superconductivity below 30 K at 83 GPa in compressed "phosphine".

Contents

S1 Computational Details

Crystal structure prediction was carried out using density functional theory (DFT) coupled with the evolutionary algorithm (EA), XTALOPT, release 9.[1] Duplicate structures were detected via the XTALCOMP algorithm.[2] EA runs were carried out on PH_n (n = 1-6) stoichiometries at 40, 60, 80 and 100 GPa employing 1-6 formula units (FU) within the simulation cells in a single run. The lowest enthalpy structures obtained from each search were relaxed in the pressure range of 40-100 GPa.

Geometry optimizations and electronic structure calculations were performed by using DFT as implemented in the Vienna *Ab-Initio* Simulation Package (VASP) version 5.4.1,[3] with the gradient-corrected exchange and correlation functional of Perdew-Burke-Ernzerhof (PBE).[4] In order to test the effect of long range intermolecular London dispersion interactions, the vdW-DF-optB88[5–7] exchange correlation functional was used to optimize the geometries and evaluate the enthalpies for PH_n structures between 40-100 GPa. However, it was determined that at the pressures studied the effect of vdW interactions for these types of systems is negligible for example compare Figure S3 with Figure S4, and see Figure S19. Meanwhile, the convergence test for various cutoff energy (ENCUT) and *k*-mesh are showing in Figure S1 and Figure S2, respectively. At 80 GPa the difference in the enthalpies of the $Cmmm$ and $C2/m$ PH_2 phases was 1.2 meV/atom, which is approximately equal to the level of convergence attained by our computational settings.

The projector augmented wave (PAW) method[8] was used to treat the core states, and a plane-wave basis set with an energy cutoff of 700 eV was employed. The H $1s^1$ and P $3s^2$/$3p^3$ electrons were treated explicitly using the PAW-PBE H and PAW-PBE P POTCARS, which are available in the potpaw-PBE.52.tar.gz file from the VASP repository. The k-point grids were generated using the Γ-centered Monkhorst-Pack scheme, and the number of divisions along each reciprocal lattice vector was chosen such that the product of this number with the real lattice constant was 30 Å in the structure searches, and 40-50 Å otherwise.

Phonon calculations were performed using the Quantum Espresso (QE)[9] program to obtain the dynamical matrix and the electron-phonon coupling (EPC) parameters. The phonon calculations showed that PH, $C2/m$ PH_2, $Cmmm$ PH_2, PH_4 and PH_5 were dynamically stable at 80 GPa. A calculation was not performed on PH_6 because of the computational expense: it had $P\bar{1}$ symmetry and 28 atoms in the unit cell. In the QE calculations, the H and P pseudopotentials, obtained from the QE pseudopotential library, were generated by the method of Trouiller-Martins[10] with $1s^2$ and $3s^23p^3$ valence configurations, respectively, along with the PBE generalized gradient approximation. Plane-wave basis set cutoff energies were set to 80 Ry for all systems. The Brillouin-zone sampling scheme of Methfessel-Paxton[11] using a smearing of 0.02 Ry and $18 \times 18 \times 18$ *k*-point grids were used for all calculations of PH_n phases, except a $12 \times 12 \times 12$ mesh was used for the $C2$ PH-phase at 80 GPa. Density functional perturbation theory as implemented in QE was employed for the phonon calculations. The EPC matrix elements were calculated using $2 \times 2 \times 2$ q-meshes for all of the structures at 80 GPa. The EPC parameter, λ, was calculated using a set of Gaussian broadenings in steps of 0.005 Ry from 0-0.300 Ry. The broadenings for which λ was converged to within 0.05 were between 0.015 and 0.040 Ry for all structures. The critical superconducting temperature, T_c, has been estimated using the

Allen-Dynes modified McMillan equation[12] as,

$$T_c = \frac{\omega_{\log}}{1.2}\exp\left[-\frac{1.04(1+\lambda)}{\lambda-\mu^*(1+0.62\lambda)}\right] \quad (1)$$

where $\omega_{\log}$ is the logarithmic average frequency. Because μ^* has been proposed to range from 0.083 for PH_3,[13] to 0.089 for hydrogen[14] to 0.18 for phosphorus,[15] the T_cs for a range of μ^* values are provided in Table S15.

The molecular calculations on the PH_5 dimer building block of $P\bar{1}$-PH_5 and the BH_3 dimer were performed by using the Amsterdam Density Functional (ADF) software package[16,17] and the PBE gradient density functional.[4] The basis functions on all of the atoms consisted of an all electron triple-ζ Slater-type basis set with polarization functions (TZP) from the ADF basis set library coupled with the zeroth-order relativistic approximation (ZORA).[18–20]

In the right hand side of Figure 3 in the main text we show the MO diagram of a P_2H_{10} fragment directly extracted from the $P\bar{1}$-PH_5 phase at 80 GPa. As expected, the main difference between it's geometry and that of the optimized P_2H_{10} was the P-H bond length. The shorter P-H distance in the compressed species leads to a larger orbital overlap and a slight broadening of the energy levels of the occupied MOs. As shown in the right panels of Figure 3d in the main text, the occupied DOS of the insulating solid spans a similar energy range as the molecular level diagram. The increase in the hydrogen s-character in the PDOS above $\sim$-5 eV to near the top of the valence states correlates with an increase in the contribution of the H s-orbitals to the HOMO and HOMO-1 of the P_2H_{10} molecule. However, in contrast to the molecular calculations where non-negligible phosphorus d-character was found in the HOMO to the HOMO-1, the PDOS did not reveal the mixing in of d-states below E_F.

S2 Discussion of Structures and Superconductivity

Our analysis suggests that the main role of the H_2 layers within $C2/m$ and $Cmmm$-PH_2 is to decrease the Coulomb repulsion between the P-H layers, and their contribution towards λ is minimal. This made us wonder if it would be possible to find a stable, superconducting, two-dimensional sheet comprised of four layers of (nearly) simple cubic phosphorus atoms terminated by hydrogen atoms at atmospheric conditions. Unfortunately, even though such a structure would have a $g(E_F)$ comparable to that of the PH_2 phases at 80 GPa, it would be dynamically unstable because of the geometry adopted by the phosphorus atoms: at room temperature and pressure the thermodynamically stable form of black phosphorus consists of edge-sharing six-rings in a chair-like conformation that form puckered layers.[21] A geometry optimization of an isolated layer with the P_2H stoichiometry resulted in the puckering of the phosphorus layers, and a concomitant opening of the band gap.

S3 XTALOPT Searches Details

The XTALOPT EA uses a population based pool, instead of a generation based pool. Thus, a new offspring is created as soon as another structure has finished optimizing. Tables S1 to S6 provide the size of the population of the EA searches we have carried out for various PH_n, $n = 1 - 6$, stoichiometries at the listed pressures. Note that each EA run considered 1-6 FU, but we list the total number of structures optimized for each FU separately.

Stoichiometry	Formula Units	Pressure (GPa)	Population (vdW-DF-optB88)	Population (PBE)
PH	1	40	209	58/419
	2		208	55/419
	3		208	55/419
	4		208	55/419
	5		208	55/420
	6		208	55/419
PH	1	60	267	392/309
	2		268	393/309
	3		267	394/309
	4		267	392/309
	5		267	391/308
	6		266	392/308
PH	1	80	262	181/167
	2		262	181/166
	3		262	181/166
	4		262	180/166
	5		261	180/166
	6		261	180/166
PH	1	100	176	193
	2		176	192
	3		176	192
	4		176	192
	5		175	192
	6		176	192

Table S1: The number of formula units, and the size of the population used in the evolutionary structure searches for PH at 40, 60, 80, and 100 GPa with either the optB88 or PBE functional. Multiple runs at the same pressure are separated by "/" for respective populations.

Stoichiometry	Formula Units	Pressure (GPa)	Population (vdW-DF-optB88)	Population (PBE)
PH_2	1	40	166	-
	2		145	-
	3		161	-
	4		166	-
	5		170	-
	6		166	-
PH_2	1	60	212	189
	2		213	189
	3		211	188
	4		211	188
	5		211	188
	6		212	188
PH_2	1	80	152/289/490	62/206
	2		151/288/491	49/206
	3		151/289/490	49/204
	4		150/288/490	48/205
	5		150/288/490	48/204
	6		150/288/491	49/204
PH_2	1	100	159	276
	2		158	275
	3		158	275
	4		158	276
	5		158	274
	6		158	274

Table S2: The number of formula units, and the size of the population used in the evolutionary structure searches for PH_2 at 40, 60, 80, and 100 GPa with either the vdW-DF-optB88 or PBE functional. Multiple runs at the same pressure are separated by "/" for respective populations.

Stoichiometry	Formula Units	Pressure (GPa)	Population (vdW-DF-optB88)	Population (PBE)
PH_3	1	40	188	-
	2		188	-
	3		188	-
	4		189	-
	5		188	-
	6		188	-
PH_3	1	60	212	298
	2		212	298
	3		212	298
	4		212	297
	5		212	297
	6		212	297
PH_3	1	80	276/136	149/355
	2		275/136	149/352
	3		275/135	149/352
	4		275/135	148/352
	5		275/135	148/352
	6		275/135	148/352
PH_3	1	100	291	474
	2		291	474
	3		291	476
	4		291	474
	5		290	474
	6		290	473

Table S3: The number of formula units, and the size of the population used in the evolutionary structure searches for PH_3 at 40, 60, 80, and 100 GPa with either the vdW-DF-optB88 or PBE functionals. Multiple runs at the same pressure are separated by "/" for respective populations. We have also carried out a 16-20 FU evolutionary search using a $2\times2\times1$ supercell of a 80 GPa $C2/m$ PH_3 structure as a seed. 345 structures were optimized with 16 FU, and 72 structures were optimized with 17-20 FU, but no more stable or dynamically stable geometry has been found.

Stoichiometry	Formula Units	Pressure (GPa)	Population (vdW-DF-optB88)	Population (PBE)
PH_4	1	40	183	196
	2		183	197
	3		183	196
	4		183	197
	5		182	195
	6		182	196
PH_4	1	60	219	382
	2		220	382
	3		220	382
	4		219	382
	5		219	382
	6		218	381
PH_4	1	80	174	225
	2		174	227
	3		173	227
	4		173	224
	5		173	224
	6		174	225
PH_4	1	100	234	369
	2		233	369
	3		233	369
	4		233	369
	5		233	369
	6		233	368

Table S4: The number of formula units, and the size of the population used in the evolutionary structure searches for PH_4 at 40, 60, 80, and 100 GPa with either the vdW-DF-optB88 or PBE functionals. Multiple runs at the same pressure are separated by "/" for respective populations.

Stoichiometry	Formula Units	Pressure (GPa)	Population (vdW-DF-optB88)	Population (PBE)
PH_5	1	40	202	101
	2		202	100
	3		202	100
	4		202	100
	5		202	100
	6		202	100
PH_5	1	60	278	171
	2		278	172
	3		278	171
	4		278	171
	5		278	170
	6		277	170
PH_5	1	80	170	149
	2		170	149
	3		170	149
	4		170	149
	5		169	148
	6		169	148
PH_5	1	100	195	408
	2		195	409
	3		195	408
	4		195	408
	5		195	407
	6		194	407

Table S5: The number of formula units, and the size of the population used in the evolutionary structure searches for PH_5 at 40, 60, 80, and 100 GPa with either the vdW-DF-optB88 or PBE functionals. Multiple runs at the same pressure are separated by "/" for respective populations.

Stoichiometry	Formula Units	Pressure (GPa)	Population (vdW-DF-optB88)	Population (PBE)
PH_6	1	40	164	270
	2		164	269
	3		163	269
	4		163	269
	5		163	269
	6		164	269
PH_6	1	60	219	368
	2		219	367
	3		219	367
	4		218	368
	5		219	368
	6		218	367
PH_6	1	80	208	263
	2		208	263
	3		208	262
	4		208	261
	5		207	261
	6		207	261
PH_6	1	100	176	251
	2		176	252
	3		176	251
	4		177	250
	5		176	249
	6		175	249

Table S6: The number of formula units, and the size of the population used in the evolutionary structure searches for PH_6 at 40, 60, 80, and 100 GPa with either the vdW-DF-optB88 or PBE. Multiple runs at the same pressure are separated by "/" for respective populations.

S4 CONTCARs of PH_n (n = 1-6) Phases

$C2$ PH			
1			
	2.18181313	0.00000000	0.00000000
	0.00000000	2.18179421	-0.00182604
	-1.09090657	-1.03873584	16.30367877
H P			
6 6			
Direct			
	0.09558634	0.79018648	0.57706354
	0.51852280	0.20981352	0.42293646
	0.15610881	0.60751690	0.46181191
	0.69429692	0.39248310	0.53818809
	0.91603330	0.85185896	0.46646891
	0.44956438	0.14814104	0.53353109
	0.13701509	0.83260742	0.66347140
	0.47354370	0.16739258	0.33652860
	0.20705144	0.90195246	0.79987943
	0.40717201	0.09804754	0.20012057
	0.34128232	0.03273740	0.06750335
	0.27377896	0.96726260	0.93249665

Table S7: CONTCAR of $C2$ PH primitive cell at 80 GPa including cell parameters in Å and fractional coordinates for atomic positions

$C2/m$ PH_2			
1			
	2.18513623	0.00000000	0.00000000
	-0.00064665	2.18513613	0.00000000
	0.02820701	-0.02819866	12.94550169
H P			
8 4			
Direct			
	0.49264568	0.50735432	0.36211771
	0.89051684	0.10948316	0.57658742
	0.61998984	0.61998984	0.50000000
	0.38001016	0.38001016	0.50000000
	0.88091535	0.11908465	0.40403726
	0.50735432	0.49264568	0.63788229
	0.11908465	0.88091535	0.59596274
	0.10948316	0.89051684	0.42341258
	0.50186403	0.49813597	0.91693226
	0.49813597	0.50186403	0.08306774
	0.50282988	0.49717012	0.74643817
	0.49717012	0.50282988	0.25356183

Table S8: Same as Table S7 but for $C2/m$ PH_2.

$Cmmm$ PH_2			
1			
	2.18698201	0.00000000	0.00000000
	-0.00809106	2.18696704	0.00000000
	0.00000000	0.00000000	12.94922034
H P			
8 4			
Direct			
	0.50000000	0.50000000	0.36196989
	0.87918419	0.12081581	0.58632376
	0.61997156	0.61997156	0.50000000
	0.38002844	0.38002844	0.50000000
	0.87918419	0.12081581	0.41367624
	0.50000000	0.50000000	0.63803011
	0.12081581	0.87918419	0.58632376
	0.12081581	0.87918419	0.41367624
	0.50000000	0.50000000	0.91710933
	0.50000000	0.50000000	0.08289067
	0.50000000	0.50000000	0.74642621
	0.50000000	0.50000000	0.25357379

Table S9: Same as Table S7 but for $Cmmm$ PH_2.

$P1$ PH_3			
1			
	2.18449431	0.00000000	0.00000000
	-0.00714128	2.18487443	0.00000000
	-0.01873739	-0.05093211	15.12205919
H P			
12 4			
Direct			
	0.71048981	0.50635126	0.52206148
	0.49208156	0.52262731	0.23769320
	0.72568243	0.28736380	0.24963750
	0.23308504	0.02244376	0.31996871
	0.50566554	0.29374466	0.54711456
	0.01210196	0.79604915	0.45139293
	0.09658348	0.88916164	0.57886922
	0.49715233	0.52231360	0.38629659
	0.23091568	0.02547610	0.46832663
	0.72908599	0.28296781	0.39156625
	0.10727303	0.90824443	0.19917611
	0.99705978	0.78262017	0.31611931
	0.10731380	0.90214944	0.10633609
	0.09987536	0.90009244	0.96005136
	0.10419691	0.89853390	0.67172915
	0.09897732	0.89822505	0.81807007

Table S10: Same as Table S7 but for $P1$ PH_3.

$C2/m$ PH_4			
1			
	2.18721623	0.00000000	0.00000000
	-0.00073313	2.18721611	0.00000000
	-0.15585981	-0.15591206	8.63638935
H P			
8 2			
Direct			
	0.89543067	0.89543067	0.64630631
	0.50361310	0.50361310	0.70919054
	0.38051039	0.61948961	0.50000000
	0.10456933	0.10456933	0.35369369
	0.11051839	0.11051839	0.60936741
	0.49638690	0.49638690	0.29080946
	0.88948161	0.88948161	0.39063259
	0.61948961	0.38051039	0.50000000
	0.50711969	0.50711969	0.87090821
	0.49288031	0.49288031	0.12909179

Table S11: Same as Table S7 but for $C2/m$ PH_4.

$P\bar{1}$ PH_5			
1			
	3.22365717	0.00000000	0.00000000
	1.60340802	3.04538784	0.00000000
	-0.12543619	-1.55496201	4.54748886
H P			
10 2			
Direct			
	0.28315292	0.80154460	0.00978155
	0.94511431	0.75873674	0.55456182
	0.05488569	0.24126326	0.44543818
	0.71684708	0.19845540	0.99021845
	0.17391855	0.31242869	0.13018565
	0.82608145	0.68757131	0.86981435
	0.44196723	0.38936854	0.62367857
	0.64388369	0.01326743	0.25131777
	0.35611631	0.98673257	0.74868223
	0.55803277	0.61063146	0.37632143
	0.86940993	0.24914007	0.74326103
	0.13059007	0.75085993	0.25673897

Table S12: Same as Table S7 but for $P\bar{1}$ PH_5.

$P\bar{1}$ PH_6			
1			
	2.17950920	0.00000000	0.00000000
	-0.00028791	4.38063766	0.00000000
	-0.11475302	-1.95650655	10.80087836
H P			
24 4			
Direct			
	0.10611396	0.98535050	0.39603435
	0.99110371	0.87370401	0.23388602
	0.00139215	0.64552380	0.76935095
	0.87848388	0.46788828	0.59350222
	0.87876871	0.41789875	0.41090455
	0.38587581	0.69453632	0.29759413
	0.39399260	0.43678761	0.71412687
	0.62613079	0.16237641	0.48383632
	0.13479431	0.13449265	0.61178652
	0.62207552	0.77975510	0.67849312
	0.38915005	0.28198952	0.49903547
	0.59817203	0.10868687	0.28656199
	0.12151612	0.53211172	0.40649778
	0.99860785	0.35447620	0.23064905
	0.00889629	0.12629599	0.76611398
	0.89388604	0.01464950	0.60396565
	0.86520569	0.86550735	0.38821348
	0.37792448	0.22024490	0.32150688
	0.40182797	0.89131313	0.71343801
	0.61084995	0.71801048	0.50096453
	0.12123129	0.58210125	0.58909545
	0.61412419	0.30546368	0.70240587
	0.37386921	0.83762359	0.51616368
	0.60600740	0.56321239	0.28587313
	0.99298650	0.80419079	0.10471155
	0.00670356	0.69912499	0.89852349
	0.99329644	0.30087501	0.10147651
	0.00701350	0.19580921	0.89528845

Table S13: Same as Table S7 but for $P\bar{1}$ PH_6.

$C2$ PH_5			
1			
	2.22811038	0.00000000	0.00000000
	0.00000000	2.23023758	0.00000000
	-1.04605431	-1.11511879	10.17687377
H P			
10 2			
Direct			
	0.23315370	0.64520572	0.35494083
	0.76684630	0.29026489	0.64505917
	0.28879006	0.75832222	0.58207087
	0.37379581	0.97097554	0.74984888
	0.62620419	0.22112667	0.25015112
	0.71120994	0.17625134	0.41792913
	0.10204036	0.83532622	0.30447563
	0.25819132	0.96352804	0.53037953
	0.89795964	0.53085059	0.69552437
	0.74180868	0.43314851	0.46962047
	0.44045645	0.03064808	0.88772573
	0.55954355	0.14292235	0.11227427

Table S14: Same as Table S7 but for $C2$ PH_5 at 60 GPa.

S5 Convergence Tests

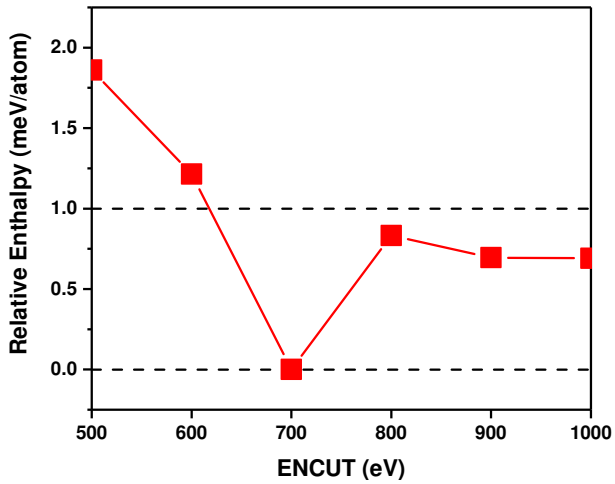

Figure S1: Relative enthalpy of the $C2/m$-PH_2 phase at 80 GPa as a function of the cutoff energy used in the plane wave basis set (ENCUT). The relative enthalpy is given with respect to the enthalpy calculated using ENCUT = 700 eV. The k-mesh used a spacing of $2\pi\times0.02$ Å^{-1}.

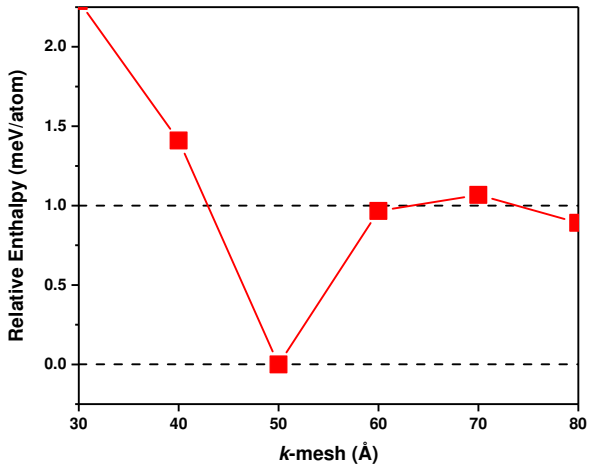

Figure S2: The relative enthalpy of the $C2/m$-PH_2 phase at 80 GPa as a function of the product of divisions along each reciprocal lattice vector with the real lattice constant. The relative enthalpy is given with respect to the enthalpy calculated with a k-mesh which used a spacing of $2\pi\times0.02$ Å^{-1}. The ENCUT employed for all calculations was 700 eV.

S6 Tie-lines

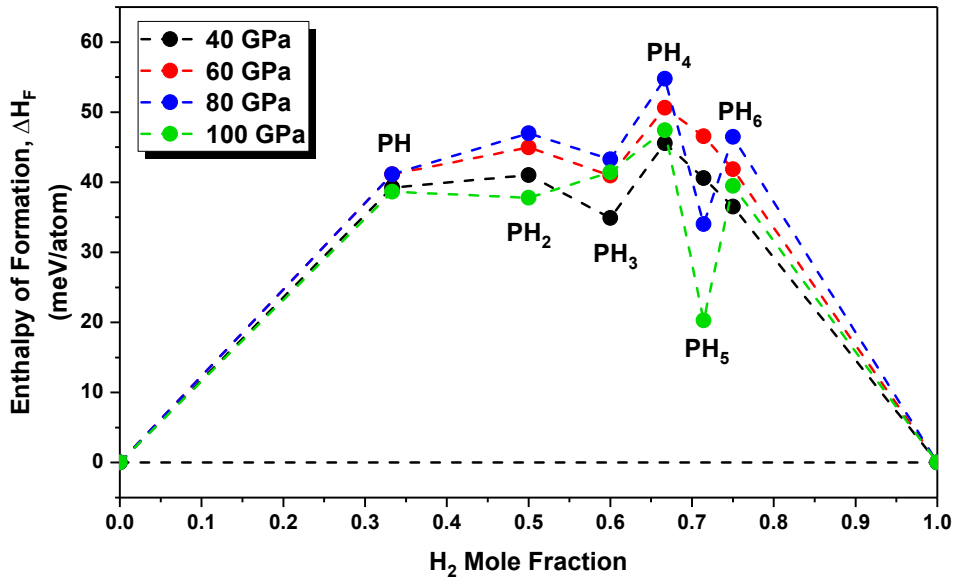

Figure S3: ΔH_F for the reaction P + $\frac{n}{2}$ H_2 $\rightarrow$ PH_n versus the H_2 mole fraction at 40, 60, 80 and 100 GPa obtained with the PBE functional.

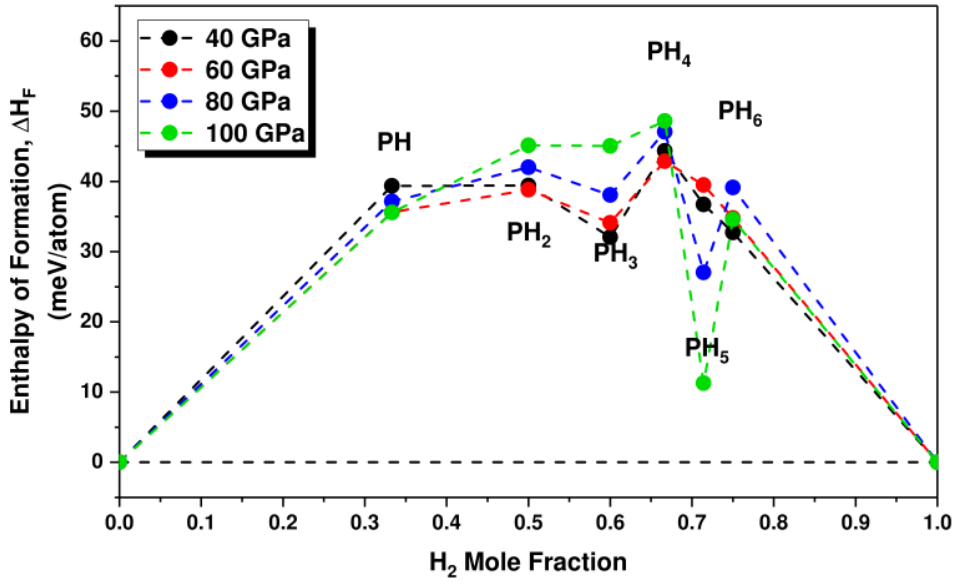

Figure S4: ΔH_F for the reaction P + $\frac{n}{2}$ H_2 $\rightarrow$ PH_n versus the H_2 mole fraction at 40, 60, 80 and 100 GPa obtained with the vdW-DF-optB88 functional.

S7 Electronic Band Structure and Density of States Plots

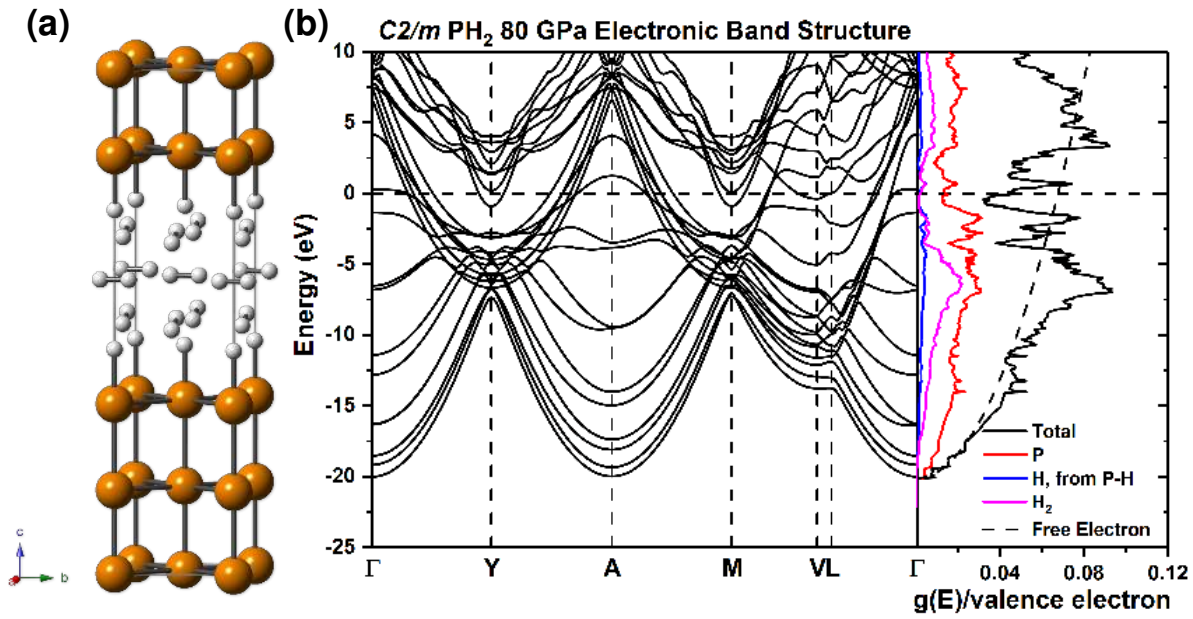

Figure S5: (a) The conventional cell of the $C2/m$ PH_2 structure at 80 GPa. Phosphorus atoms are orange; hydrogen atoms are white. (b) Electronic band structure along with the total and site projected electronic DOS of $C2/m$-PH_2 at 80 GPa. E_F is set to zero.

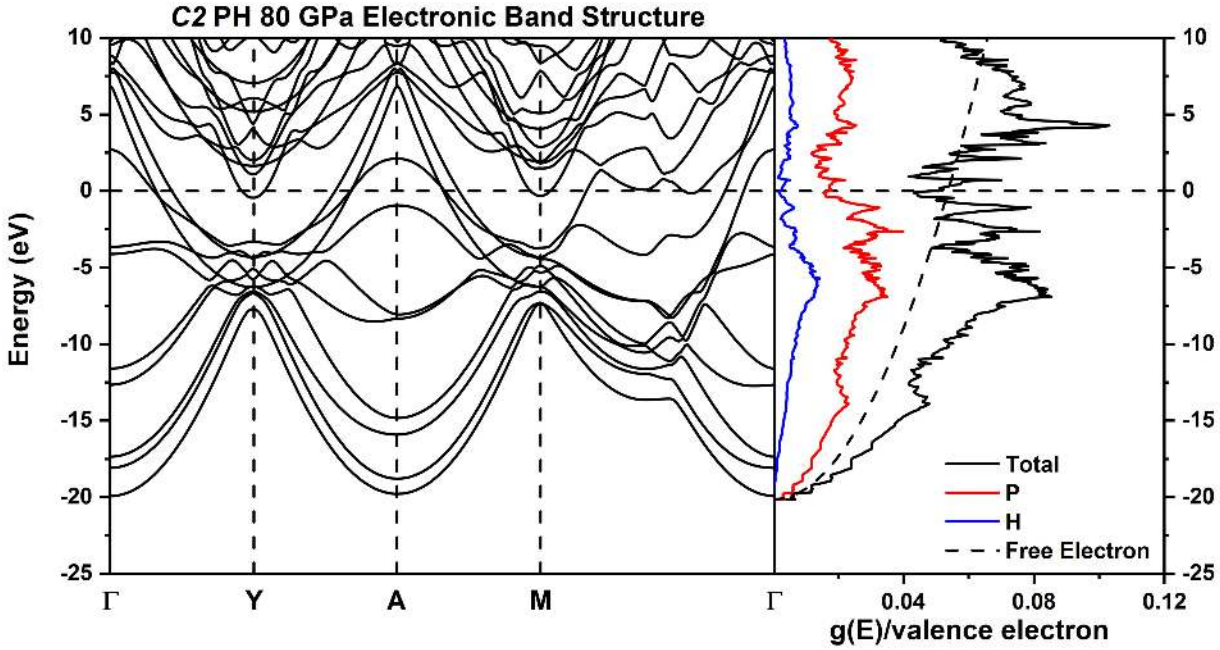

Figure S6: Electronic band structure along with the total and site projected electronic DOS of Cm-PH at 80 GPa. E_F is set to zero.

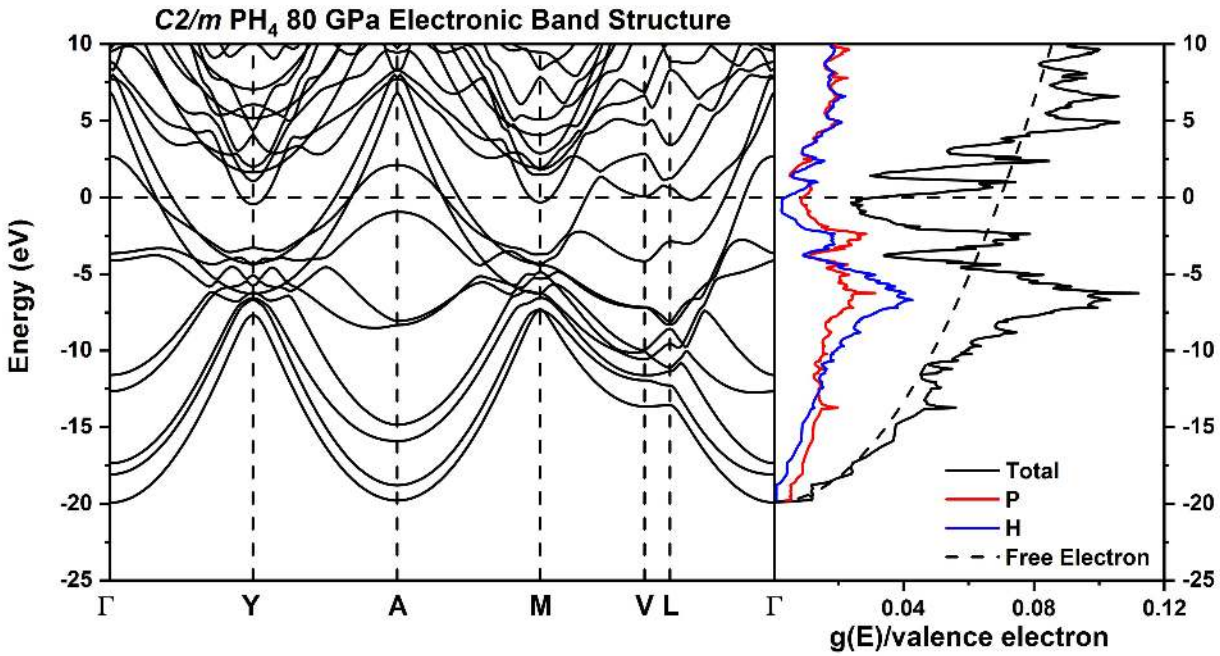

Figure S7: Electronic band structure along with the total and site projected electronic DOS of $C2/m$-PH_4 at 80 GPa. E_F is set to zero.

S8 Electron-Phonon Coupling and Superconductivity

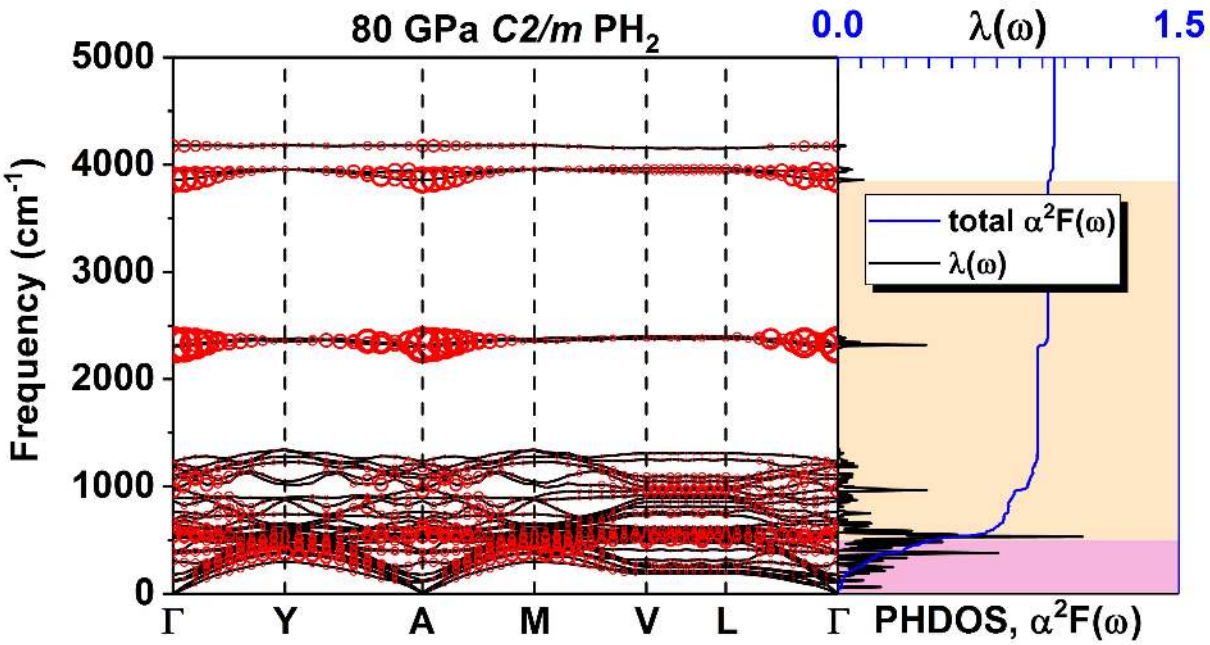

Figure S8: Phonon band structure, Eliashberg spectral function, $\alpha^2F(\omega)$, and the electron-phonon integral, $\lambda(\omega)$ for $C2/m$ PH_2 at 80 GPa. Circles indicate the phonon line width with a radius proportional to the strength. The highlighted sections of the $\alpha^2F(\omega)$ plots show the division into vibrational modes that are comprised of phosphorus vibrations (P-P, pink), motions of hydrogen and phosphorus atoms (P-H, tan), and mainly hydrogen vibrations (H-H, white). The contribution towards λ for these divisions are 0.41 (43.3%), 0.51 (53.8%), and 0.03 (2.9%) for the pink, tan, and white divisions, respectively.

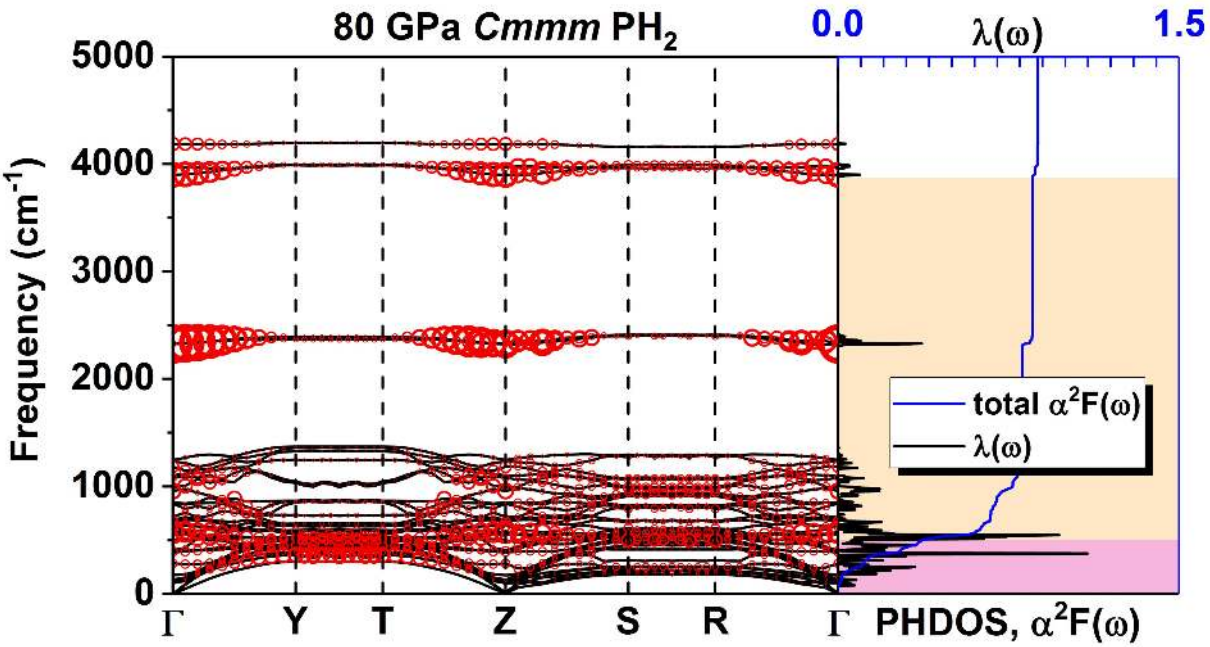

Figure S9: Phonon band structure, Eliashberg spectral function, $\alpha^2F(\omega)$, and the electron-phonon integral, $\lambda(\omega)$ for $Cmmm$ PH_2 at 80 GPa. Circles indicate the phonon line width with a radius proportional to the strength. The highlighted sections of the $\alpha^2F(\omega)$ plots show the division into vibrational modes that are comprised of phosphorus vibrations (P-P, pink), motions of hydrogen and phosphorus atoms (P-H, tan), and mainly hydrogen vibrations (H-H, white). The contribution towards λ for these divisions are 0.37 (42.0%), 0.48 (55.3%), and 0.02 (2.7%) for the pink, tan, and white divisions, respectively.

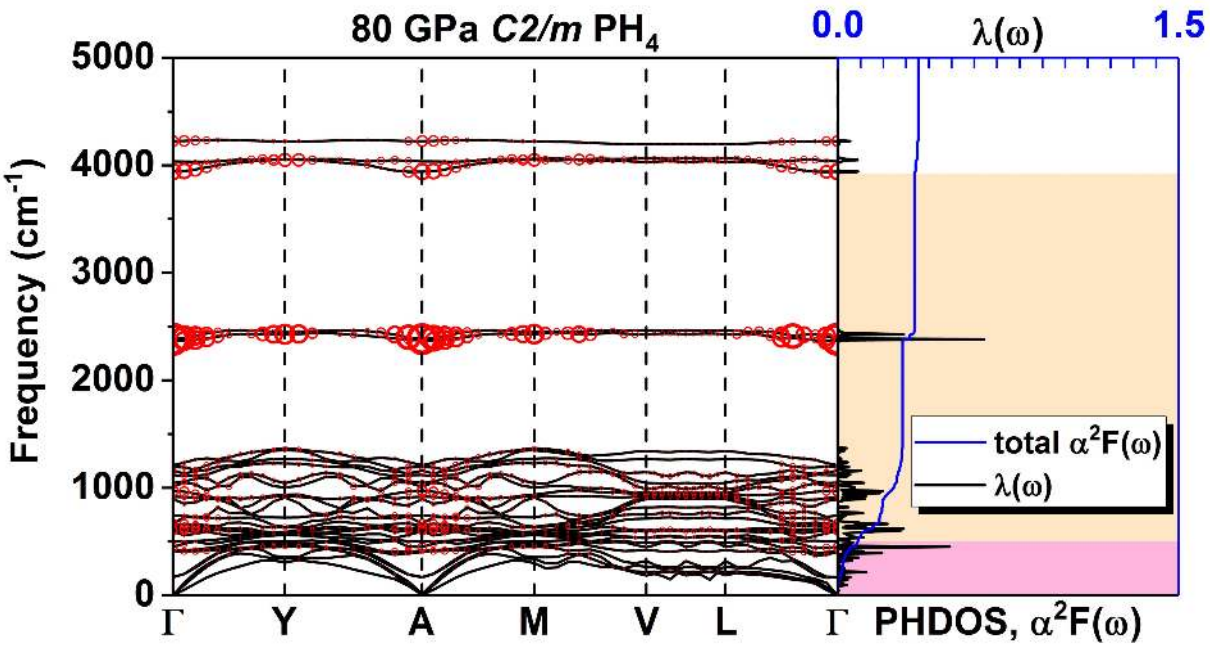

Figure S10: Phonon band structure, Eliashberg spectral function, $\alpha^2F(\omega)$, and the electron-phonon integral, $\lambda(\omega)$ for $C2/m$ PH_4 at 80 GPa. Circles indicate the phonon line width with a radius proportional to the strength. The highlighted sections of the $\alpha^2F(\omega)$ plots show the division into vibrational modes that are comprised of phosphorus vibrations (P-P, pink), motions of hydrogen and phosphorus atoms (P-H, tan), and mainly hydrogen vibrations (H-H, white). The contribution towards λ for these divisions are 0.08 (24.5%), 0.24 (70.7%), and 0.02 (4.8%) for the pink, tan, and white divisions, respectively.

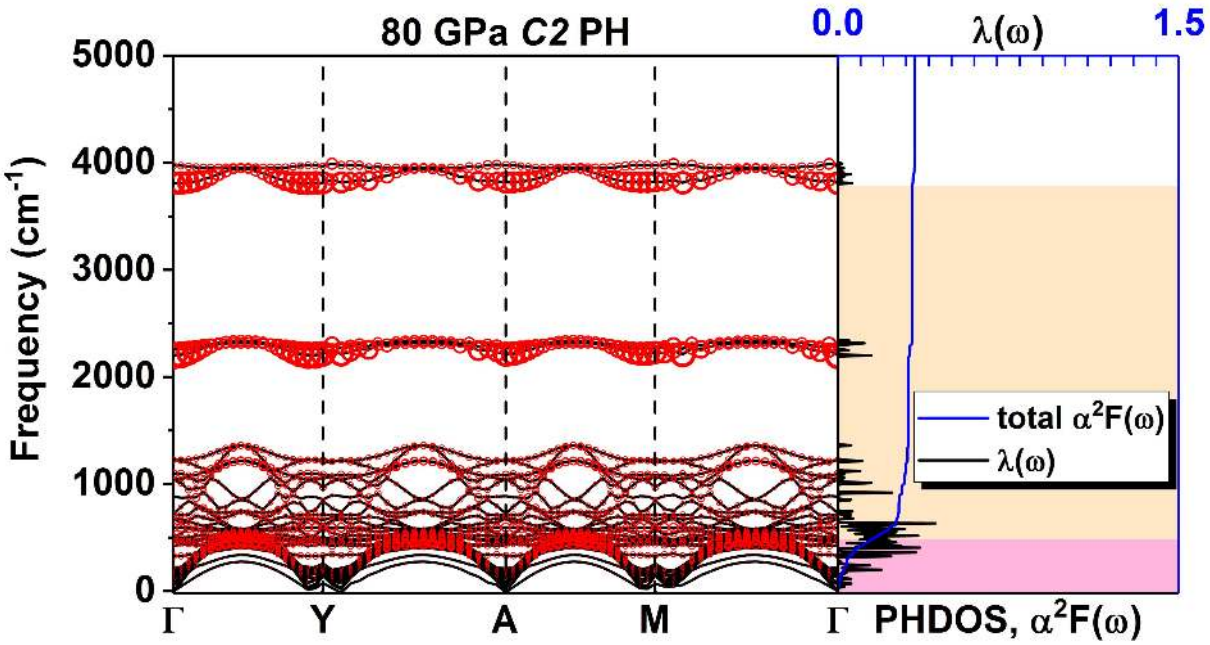

Figure S11: Phonon band structure, Eliashberg spectral function, $\alpha^2F(\omega)$, and the electron-phonon integral, $\lambda(\omega)$ for $C2$ PH at 80 GPa. Circles indicate the phonon line width with a radius proportional to the strength. The highlighted sections of the $\alpha^2F(\omega)$ plots show the division into vibrational modes that are comprised of phosphorus vibrations (P-P, pink), motions of hydrogen and phosphorus atoms (P-H, tan), and mainly hydrogen vibrations (H-H, white). The contribution towards λ for these divisions are 0.28 (43.9%), 0.33 (52.9%), and 0.02 (3.2%) for the pink, tan, and white divisions, respectively.

Table S15: Electron-phonon coupling parameter (λ), logarithmic average of phonon frequencies ($\omega_{\log}$) and estimated superconducting critical temperature (T_c) for values of the Coulomb pseudopotential (μ^*) of 0.08-0.18 for simple cubic (S.C.) phosphorus, the $C2$ PH, $C2/m$ PH_2, $Cmmm$ PH_2, and the $C2/m$ PH_4 phases at 80 GPa.

System	λ	$\omega_{\log}$ (K)	$T_c^{\mu^*=0.08}$ (K)	$T_c^{\mu^*=0.10}$ (K)	$T_c^{\mu^*=0.18}$ (K)
S.C. P	0.70	528.2	21.6	18.5	8.2
$C2$ PH	0.63	476.7	14.9	12.3	4.4
$C2/m$ PH_2	0.95	467.2	33.2	30.1	18.4
$Cmmm$ PH_2	0.88	529.4	33.0	29.5	16.9
$C2/m$ PH_4	0.34	683.2	3.1	1.9	0.0

S9 8 Formula Unit (FU) PH_2

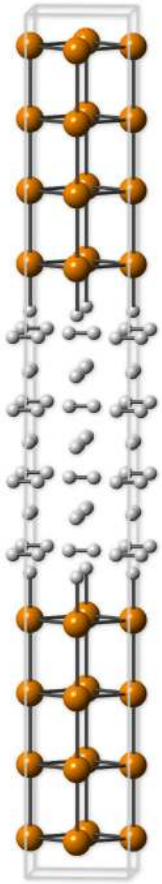

Figure S12: The conventional cell of an 8 FU PH_2 structure at 80 GPa. Phosphorus atoms are orange; hydrogen atoms are white. The structure is created by doubling the unit cell of the 4 FU $C2/m$ PH_2 structure along the c-axis. The thickness of phosphorus and H_2 layers are also doubled. The enthalpy (ΔH_F) of formation for this structure with respect to decomposition into elemental P and H phases is 33.5 meV/atom, and the 8 FU PH_2 structure is 12.7 meV/atom more stable than the most stable 4 FU PH_2 phase. It is not surprising that the structure with the thicker P/H_2 layers is enthalpically more stable. Because the phosphorus polyhydride phases are thermodynamically unstable with respect to decomposition into solid elemental H_2 and phosphorus at these pressures, an evolutionary run should, in principle, evolve towards a structure with infinitely thick P/H_2 layers in the limits of infinte cell size.

S10 Electron Localization Functions and Bader Analysis of $C2/m$ PH_2 and its Modifications

Table S16: The Average Bader Charges Per Atom Type.

System	P (1) (e)	P (2) (e)	H (1) (e)	H (2) (e)	H (3) (e)
P_2H	0.21	-0.02/0.07	-0.24	–	–
P_2H (Staggered)	0.24	0.02	-0.26	–	–
PH	0.40	-0.05/0.04	-0.40	–	-0.04/0.04
PH (H_2 shifted)	0.35	-0.03/0.06	-0.37	–	-0.04/0.03
P_2H_3	0.19	0.04	-0.23	-0.04/0.03	–
$C2/m$ PH_2	0.38	-0.03/0.06	-0.40	-0.02/0.02	-0.03/0.03
P_2H_5	0.43	-0.09/0.08	-0.43	-0.01/0.01	-0.01/0.01
$Cmmm$ PH_2	0.38	-0.04/0.06	-0.39	-0.03/0.03	-0.03/0.03

P (1) is for the P atoms bonded to H atoms (P-H); P (2) is for the P atoms only participating in P-P bonds; H (1) is for the H atoms bonded to P atoms (P-H); H (2) is for the H atoms in the top and bottom H_2 layers; H (3) is for the H atoms in the middle H_2 layers.

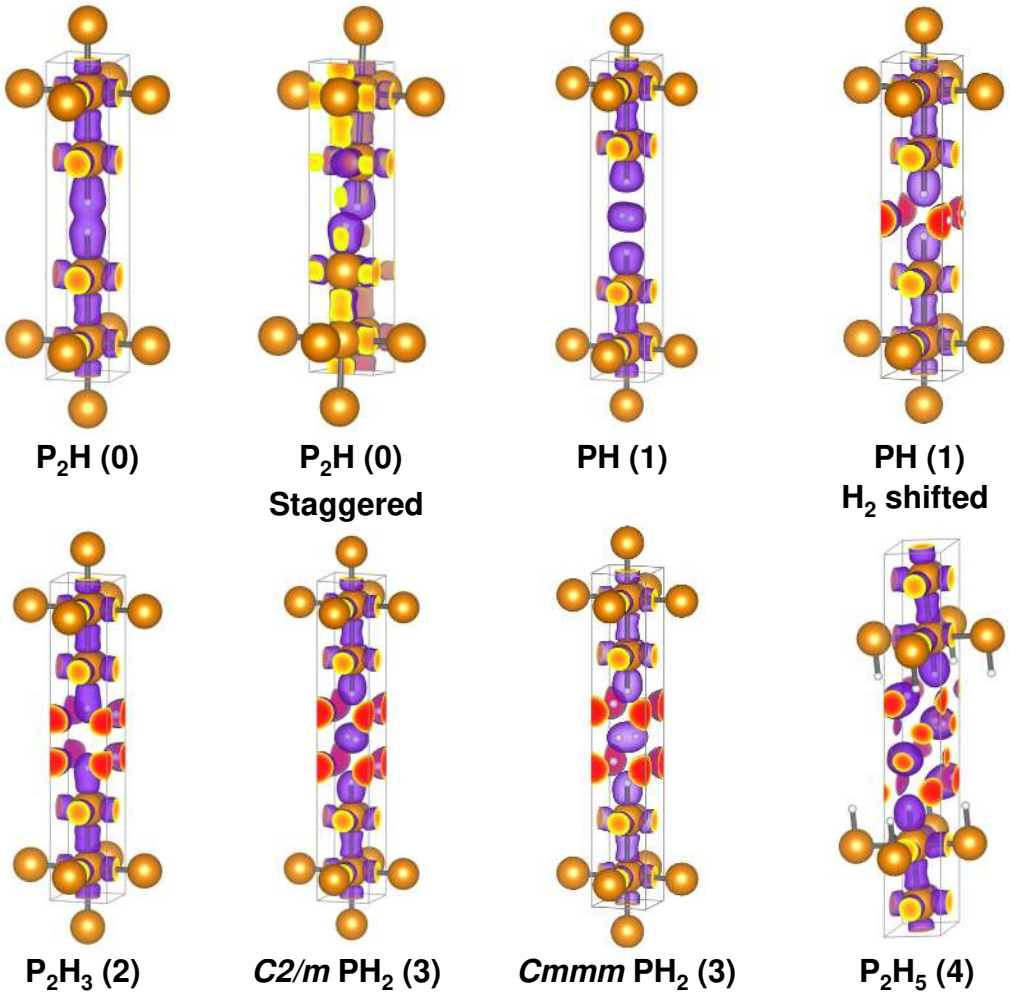

Figure S13: The isosurface (ELF=0.7) of the electron localization function of $C2/m$ PH_2, its modifications and $Cmmm$ PH_2 at 80 GPa. The number in brackets is the number of H_2 layers present in the structure.

S11 Nudged Elastic Band Calculations (NEB)

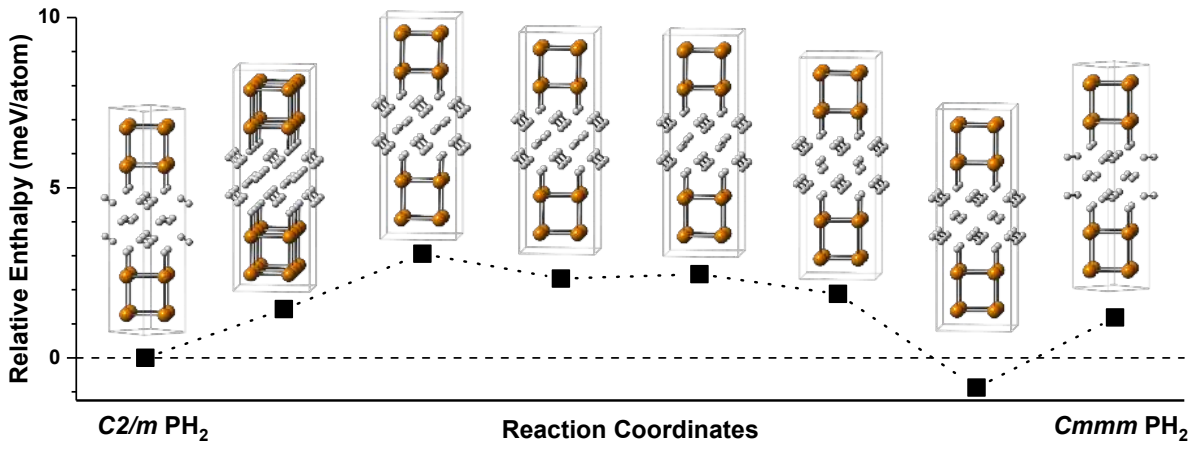

Figure S14: Calculated NEB barrier plot of one pathway connecting the $C2/m$ PH_2 and the $Cmmm$ PH_2 phases where the enthalpies are provided relative to the enthalpy of the $C2/m$ PH_2 structure at 80 GPa.

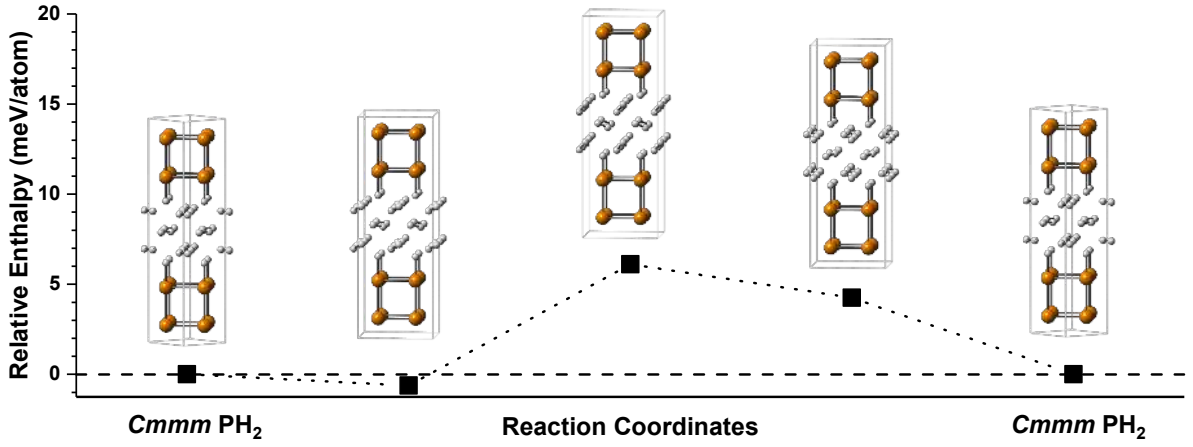

Figure S15: Calculated NEB barrier plot with all H_2 rotating 180° where the enthalpies are provided relative to the enthalpy of the $Cmmm$ PH_2 structure at 80 GPa.

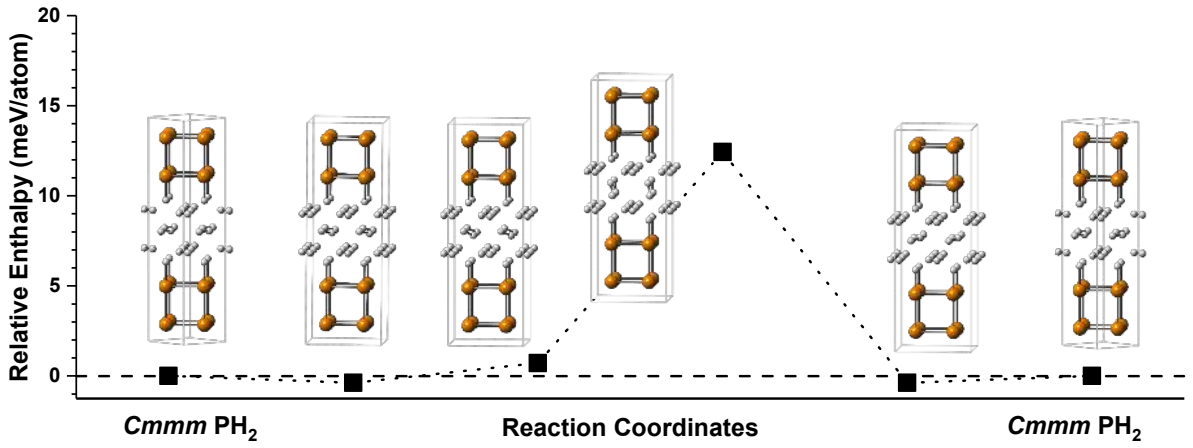

Figure S16: Calculated NEB barrier plot with only middle layers of H_2 rotating 180° where the enthalpies are provided relative to the enthalpy of the $Cmmm$ PH_2 structure at 80 GPa.

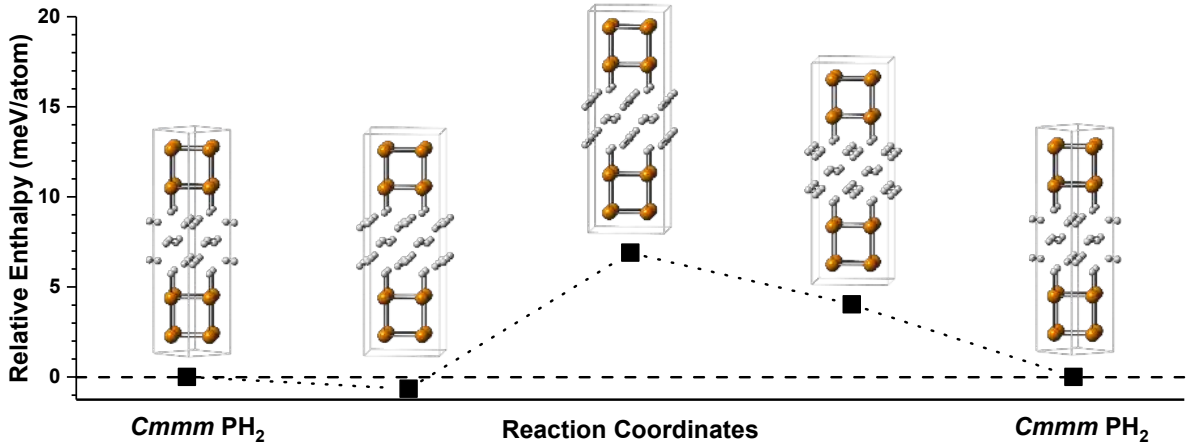

Figure S17: Calculated NEB barrier plot with only side layers of H_2 rotating 180° where the enthalpies are provided relative to the enthalpy of the $Cmmm$ PH_2 structure at 80 GPa.

S12 Structures Extracted from the *ab initio* Molecular Dynamics Simulations

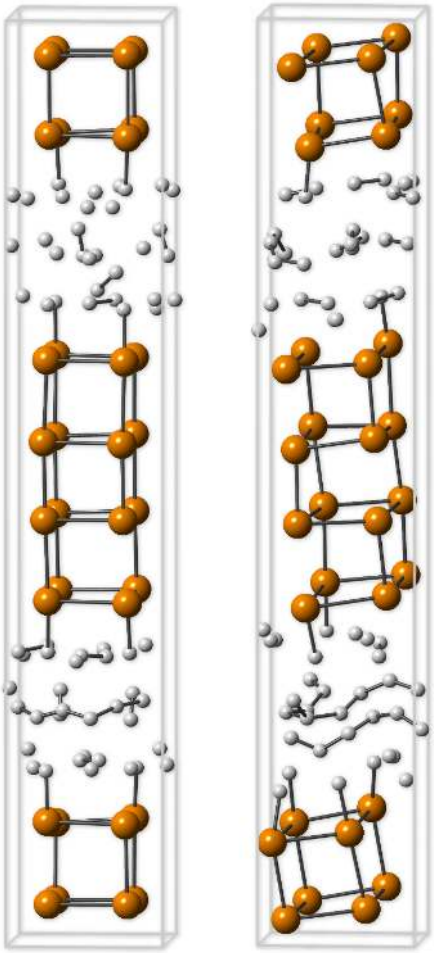

Figure S18: Snap shots of a couple of structures obtained during the *ab initio* molecular dynamics calculations as examples to illustrate the formation of extended hydrogenic lattices that result from the rotation of molecular hydrogen within the layers. Both of these two structures are obtained from the simulation at 100 K and the cutoff distance for the H-H bonds was chosen to be 1.0 Å.

S13 PH_5

S13.1 Phase Transition

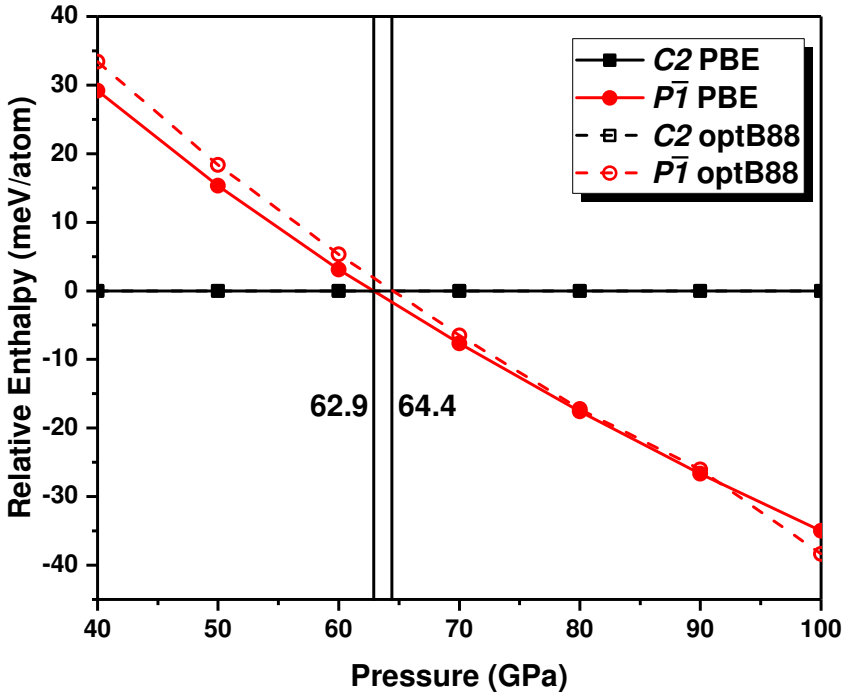

Figure S19: The enthalpies as a function of pressure for the $P\bar{1}$ phase of PH_5 relative to a $C2$ phase between 40 and 100 GPa. Solid lines are results obtained with the PBE functional; dashed lines are results obtained with the vdW-DF-optB88 functional.

S13.2 Phonon Band Structure and Density of States

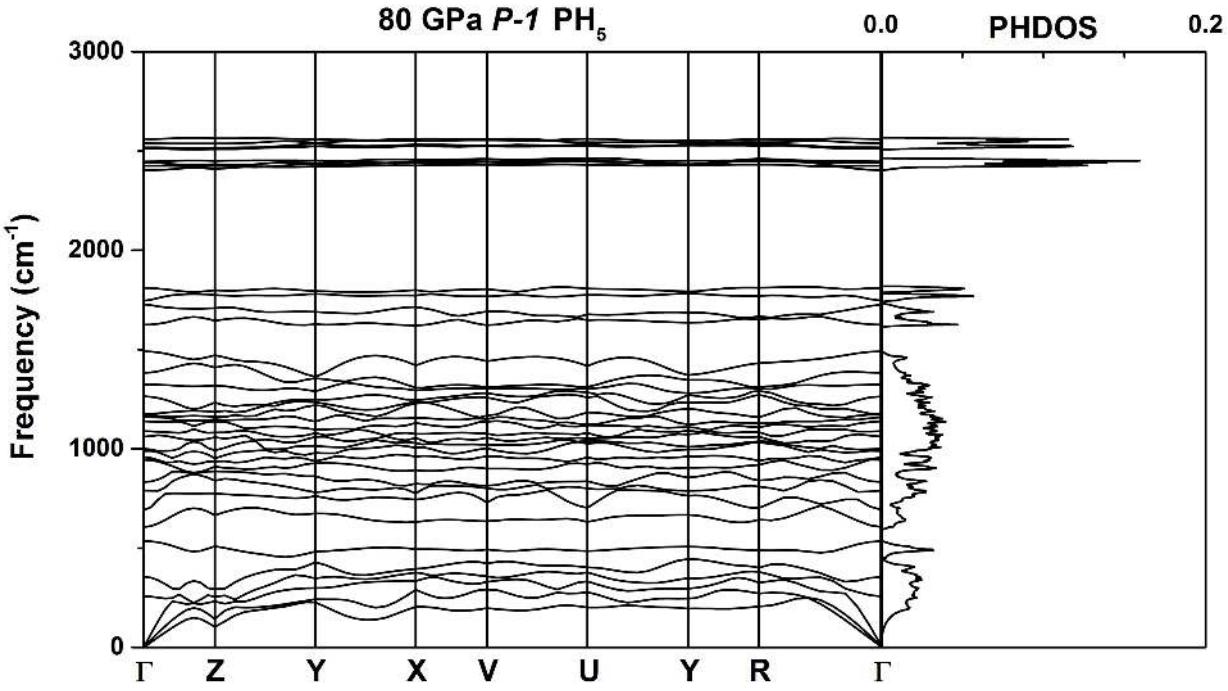

Figure S20: The phonon band structure and phonon density of states plot for $P\bar{1}$ PH_5 at 80 GPa.

S13.3 PH_5 Electronic Localization Function

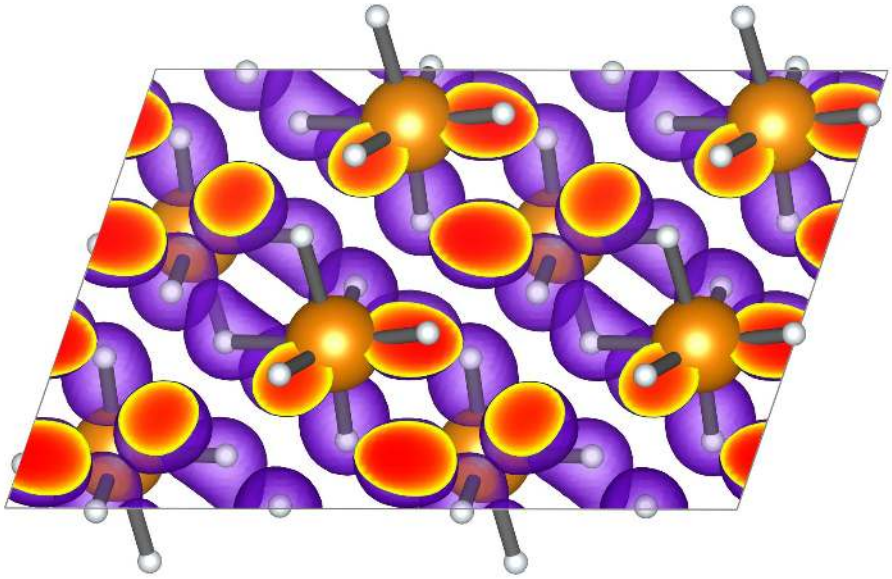

Figure S21: An isosurface (ELF=0.7) of the electron localization function of the $P\bar{1}$ PH_5 at 80 GPa.

References

[1] Z. Falls, D. C. Lonie, P. Avery, A. Shamp, E. Zurek, *Comput. Phys. Commun.* **2016**, *199*, 178–179.

[2] D. C. Lonie, E. Zurek, *Comput. Phys. Commun.* **2012**, *183*, 690–697.

[3] G. Kresse, J. Hafner, *Phys. Rev. B* **1993**, *47*, 558.

[4] J. P. Perdew, K. Burke, M. Ernzerhof, *Phys. Rev. Lett.* **1996**, *77*, 3865–3868.

[5] J. Klimeš, D. R. Bowler, A. Michaelides, *Phys. Rev. B* **2011**, *83*, 195131.

[6] M. Dion, H. Rydberg, E. Schröder, D. C. Langreth, B. I. Lundqvist, *Phys. Rev. Lett.* **2004**, *92*, 246401.

[7] G. Román-Pérez, J. M. Soler, *Phys. Rev. Lett.* **2009**, *103*, 096102.

[8] P. E. Blöchl, *Phys. Rev. B* **1994**, *50*, 17953–17979.

[9] P. Giannozzi, S. Baroni, N. Bonini, M. Calandra, R. Car, C. Cavazzoni, D. Ceresoli, G. L. Chiarotti, M. Cococcioni, I. Dabo, *J. Phys.: Condens. Matter.* **2009**, *21*, 395502.

[10] N. Troullier, J. L. Martins, *Phys. Rev. B* **1991**, *43*, 1993–2006.

[11] M. Methfessel, A. T. Paxton, *Phys. Rev. B* **1989**, *40*, 3616–3621.

[12] P. B. Allen, R. Dynes, *Phys. Rev. B* **1975**, *12*, 905.

[13] A. P. Durajski, *Sci. Rep.* **2016**, *6*, 38570.

[14] J. M. McMahon, D. M. Ceperley, *Phys. Rev. B* **2011**, *84*, 144515.

[15] K. T. Chan, B. D. Malone, M. L. Cohen, *Phys. Rev. B* **2013**, *88*, 064517.

[16] E. J. Baerends, T. Ziegler, A. J. Atkins, J. Autschbach, D. Bashford, A. Bérces, F. M. Bickelhaupt, C. Bo, P. M. Boerritger, L. Cavallo, D. P. Chong, D. V. Chulhai, L. Deng, R. M. Dickson, J. M. Dieterich, D. E. Ellis, M. van Faassen, A. Ghysels, A. Giammona, S. J. A. van Gisbergen, A. W. Götz, S. Gusarov, F. E. Harris, P. van den Hoek, C. R. Jacob, H. Jacobsen, L. Jensen, J. W. Kaminski, G. van Kessel, F. Kootstra, A. Kovalenko, M. Krykunov, E. van Lenthe, D. A. McCormack, A. Michalak, M. Mitoraj, S. M. Morton, J. Neugebauer, V. P. Nicu, L. Noodleman, V. P. Osinga, S. Patchkovskii, M. Pavanello, C. A. Peeples, P. H. T. Philipsen, D. Post, C. C. Pye, W. Ravenek, J. I. Rodríguez, P. Ros, R. Rüger, P. R. T. Schipper, H. van Schoot, G. Schreckenbach, J. S. Seldenthuis, M. Seth, J. G. Snijders, M. Solà, M. Swart, D. Swerhone, G. te Velde, P. Vernooijs, L. Versluis, L. Visscher, O. Visser, F. Wang, T. A. Wesolowski, E. M. van Wezenbeek, G. Wiesenekker, S. K. Wolff, T. K. Woo, A. L. Yakovlev, *ADF2016, SCM, Theoretical Chemistry, Vrije Universiteit, Amsterdam, The Netherlands, https://www.scm.com*.

[17] G. te Velde, F. M. Bickelhaupt, E. J. Baerends, C. Fonseca Guerra, S. J. A. van Gisbergen, J. G. Snijders, T. Ziegler, *J. Comput. Chem.* **2001**, *22*, 931–967.

[18] E. van Lenthe, E.-J. Baerends, J. G. Snijders, *J. Chem. Phys.* **1993**, *99*, 4597–4610.

[19] E. van Lenthe, E.-J. Baerends, J. G. Snijders, *J. Chem. Phys.* **1994**, *101*, 9783–9792.

[20] E. van Lenthe, A. Ehlers, E.-J. Baerends, *J. Chem. Phys.* **1999**, *110*, 8943–8953.

[21] A. Brown, S. Rundqvist, *Acta Crystallogr.* **1965**, *19*, 684–685.